Original Article

JCBFM

Journal of Cerebral Blood Flow & Metabolism
2017, Vol. 37(2) 444–455

DOI: 10.1177/0271678X16629485
jcbfm.sagepub.com
SAGE

Normalised time-to-peak-distribution curves correlate with cerebral white matter hyperintensities – Could this improve early diagnosis?

Christian Nasel[1,2,3], Roland Boubela[2,3], Klaudius Kalcher[2,3] and Ewald Moser[2,3]

Abstract

Parameter-free assessment of the time-to-peak (TTP) histogram, termed 'TTP-distribution curve' (TDC), of dynamic susceptibility contrast-enhanced magnetic resonance imaging (DSC-MRI) was introduced as a robust method to evaluate cerebral perfusion. TDC-assessment works fully automatically without the need of an arterial input function, thereby providing full comparability between different measurements. In the investigated sample of 106 patients, a strong dependency of TDC on the hemodynamic state of cerebral microvessels and the arterio-venous bolus-transit time $\boldsymbol{T_{av}}$ was demonstrated. Accordingly, TDC-derived $\boldsymbol{T_{av}}$ was 3.3–3.7 s for control patients and 4.4 s for cerebral small vessel disease patients. Measurements of associated bolus spread velocities v and accelerations $\vec{a}$ additionally revealed a direct effect from spin–spin relaxation time T_2-weighted white matter hyperintensity volume, considered to indicate microangiopathy in cerebral small vessel disease, on the TDC-measurements. This strongly supports the prevailing hypothesis that cerebral small vessel disease directly influences DSC-measurements, where the degree could be estimated from an analysis of TDC. While this may be used to correct DSC-parameters for undesirable effects from cerebral small vessel disease, it could also serve to potentially identify patients at risk for cerebral small vessel disease at an early stage, since a subset of patients without yet significant WHM-volume, but clearly altered hemodynamics in TDC-measurements, was identified in this study.

Keywords

Brain perfusion, cerebral small vessel disease, leukoaraiosis, perfusion imaging, perfusion magnetic resonance imaging

Received 20 October 2015; Revised 12 December 2015; Accepted 3 January 2016

Introduction

Recently, the analysis of the time-to-peak (TTP) histogram of dynamic susceptibility contrast-enhanced magnetic resonance imaging (DSC-MRI), termed as 'TTP-distribution curve' (TDC), was reported to detect hemodynamically meaningful variances of the individual cerebral bolus transit time.[1] Most of the routinely used DSC-MRI-derived hemodynamic parameters, e.g. mean transit time, TTP, relative TTP, standardised TTP and T_{max}, depend on the cerebral bolus transit time, which is a quantity of the mean arterio-venous transit time.[2,3] In comparison to these parameters, it seems noteworthy that for TDC-based evaluations, no specific assumptions have been used except few basic physiological facts, i.e. that the blood is entering the brain from the arterial side, passing the parenchyma, and leaving via the venous branches. Investigations of the TDC revealed considerable variations of the individual cerebral bolus transit time even in control patients, which are not yet fully

[1]Department of Radiology, University Hospital Tulln, Karl Landsteiner University of Health Sciences, Tulln, Austria
[2]Center for Medical Physics and Biomedical Engineering, Medical University of Vienna, Vienna, Austria
[3]MR Center of Excellence, Medical University of Vienna, Vienna, Austria

Corresponding author:
Christian Nasel, Department of Radiology, University Hospital Tulln, Karl Landsteiner University of Health Sciences, Alter Ziegelweg 10 A – 3430 Tulln, Austria.
Email: christian.nasel@meduniwien.ac.at

understood. According to a previous report, most of the encountered variability of the cerebral hemodynamics seems to relate to alterations in cerebral microvessels, namely arterioles, capillaries and venules.[1] As TDC appeared quite sensitive to hemodynamic alterations triggered within these vessel segments, this could lead to a novel approach to investigate the state of cerebral small vessels on the one hand, and to correct DSC-derived perfusion parameters for degenerative vascular adaptions of the arterio-venous transit time on the other hand. Therefore, we specifically investigated the relation between TDC-derived parameters (i.e. bolus transit time $\boldsymbol{T}$, bolus spread velocity $\boldsymbol{v}$ and bolus spread acceleration $\bar{\boldsymbol{a}}$) and the extent of correlated T_2-weighted white matter hyperintensities (WMH) primarily attributable to cerebral small vessel disease (cSVD).[4]

Materials and methods

Patients

A random sample of 106 patients with DSC-MRI examinations of sufficient image quality showing various degrees of WMHs was drawn from our institutional database ($n =$ app. 6862 DSC-MRI examinations).[5] Only patients with various degrees of leukoaraiosis and/or lacunar infarctions < 20 mm were eligible, while subjects presenting with circumscribed acute or chronic lesions, such as tumor, hemorrhage, thromboembolic infarcts (non-subcortical, > 20 mm), vascular malformations, inflammations, etc. were excluded. Although within the spectrum of cSVD, patients depicting signs of small lobar hemorrhages were also excluded from further analysis in order to reduce the overlap with cerebral amyloid angiopathy. Subjects suspected to suffer rare hereditary forms of cSVD (e.g. CADASIL, COL4A1-mutations) as well as patients with known chronic heart failure according to New York Heart Association (NYHA) class IV were also not included in the study. Written informed consent was obtained from all patients. The study was approved by the Lower Austrian Ethics Commission (GS4-EK-4/220-2013). All patients and data were handled following the WMA-recommendations of ethical principles for medical research involving human subjects.[6]

Magnetic resonance imaging and assessment environment

All examinations were performed on a clinical 1.5T MR-scanner (Avanto, Siemens Medical Systems, Erlangen, Germany) according to our standard perfusion-MRI protocol, which consisted of DSC-MRI, diffusion weighted MRI (dual-b SE-EPI: $b1 = 0$ s/mm^2; $b2 = 1000$ s/mm^2), MR-angiography and conventional MRI including enhanced proton density (PD)/T2w-IR-imaging.[7] Specifically, DSC-MRI was performed using a short-TR dynamic contrast-enhanced T_2^*-weighted single shot GRE-EPI-sequence (TR = 689 ms/ TE = 17 ms/FOV = 240 mm/ slice thickness: 6 mm/ image matrix: 164×208 voxels) that allowed acquisition of 81 image-stacks, with 20 slices each, at a scan time of approx. 60 s. This MRI-sequence offers an acceptable trade-off between sufficient signal-to-noise and high temporal resolution, which in turn enables critical sampling of the first pass of the administered contrast bolus through the brain at a sampling rate of 1.45 Hz for an expected minimal arterio-venous contrast bolus-transit time of about 3.5 s for regular perfusion.[8,9] During the perfusion sequence a bolus of 0.1 mmol/kg$_{(\text{body weight})}$ of MR-contrast medium, either Gadoteridol or Gadoterate meglumine was injected into a cubital vein via a 20-gauge venous cannula. All injections were performed at a flow rate of 5 ml/s using an automatic contrast injector (Optistar^{TM} Elite mobile, Mallinckrodt), 10 s after the perfusion sequence was started. Additionally, 20 ml saline (flow: 3 ml/s) was injected immediately after the contrast bolus, in order to reach a sufficient venous wash out at the injection site.

Assessment of T_2-weighted white matter hyperintensities

WMH-volumes were assessed using in-house developed R-scripts together with SPM12 segmentation routines. The first echo images of the enhanced PD/T_{2w}-IR-sequence served to obtain masks for grey and white matter, which defined all voxels considered to belong to brain parenchyma. An automatically generated contrast threshold defined as: median $+ 2 \times$ MAD (median absolute deviation) was derived from this parenchyma-voxel fraction using the signal intensities from the second echo images of the enhanced PD/T_{2w}-IR-sequence. The latter images were also used to segment the WMHs. The second echo of this sequence is equivalent to extended fluid attenuated inversion recovery imaging. From this segmentation, an estimate of the absolute WMH volume was computed and subsequently normalised to the sample mean total brain volume (TBV) to avoid bias from differing absolute brain volumes. Attempting to separate presumably 'age-related' micro-vascular degeneration from advanced cSVD, the small variance of the rather low normalised WMH (nWMH) volumes in patients aged less than 53 years in our sample was striking. Visual differentiation of manifest cSVD from most likely 'age-related' degeneration via the size of the nWHM-volumes alone was impossible in these patients.

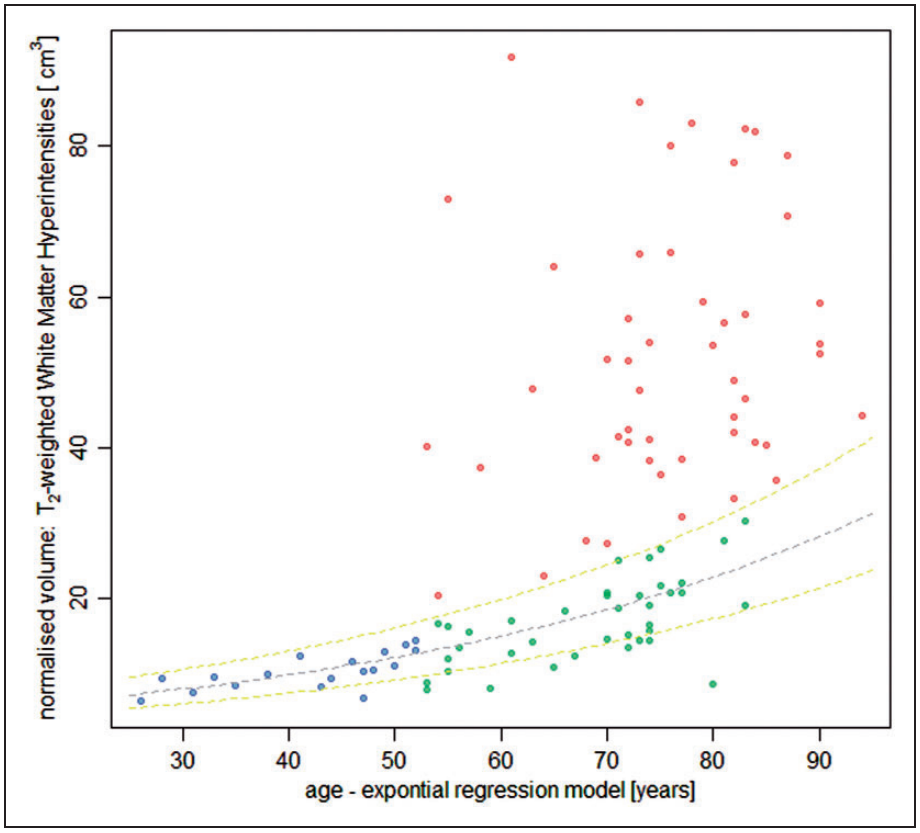

Figure 1. Using a sample-driven exponentially increasing regression model, three groups were differentiated: group 0 included young controls (age < 53 y [sample-defined], blue dots), where a differentiation of manifest cSVD from 'age-related' degeneration using nWMH-volumes was not possible. The model-derived base line (grey) and its estimated variance (yellow) are depicted as dashed lines. Patients aged ≥ 53 years with a nWMH-volume smaller or equal to the predicted upper variance-limit were judged as elderly controls (group 1, green dots), all other cases were considered as cSVD-patients (group 2, red dots).

Compared to a widely accepted visual rating scale often used in large cSVD trials, these patients resembled grade 1 at maximum of the visual scale, where a grade 1 in visual scoring is given for minimal white matter hyperintensities only.[10,11] Therefore, their nWMH-findings were considered as the most acceptable base line for the whole sample, which then defined group 0 (young control patients: $n = 18$, age < 53 years) in our study. According to investigations of WMHs attributable to cSVD and their correlation to cerebral vessel density, an exponential instead of a linear regression model was applied to extrapolate this base-line to patients aged ≥ 53 years.[12] To this end, linear regression was applied to the logarithm of the data, and regression line subsequently transformed back into the original scale. Finally, the variance of the base line was considered by adding the MAD estimated from group 0 to the exponentially increasing regression line, which allowed definition of an age-dependent threshold to additionally separate groups 1 (elderly control patients: $n = 38$, age ≥ 53 years, nWMH-volume ≤ threshold) and 2 (cSVD-patients: $n = 50$, age ≥ 53 years, nWMH-volume > threshold) (Figure 1)), both covering the same age range. Consistent with our data driven analysis, groups 0 and 1 were comparable to Fazekas grades 1 and 2 (= controls) and group 2 corresponded to Fazekas grade 3 (= cSVD patients).

Assessment of cerebral hemodynamics

Image data were anonymised and reviewed on a PC-work station using freely available and in-house developed software packages (MRIcro[13]). Perfusion images were coregistered to morphological images of the enhanced PD/T2w-IR-sequence using SPM12 (Statistical Parameter Mapping 12, UCL-Wellcome Trust Centre for Neuroimaging). The time-to-peak histogram or TDC, respectively, of each DSC-examination was provided by full-automatic calculation of standardised time-to-peak (stdTTP) parameter maps using in-house developed software (jPerfusion Module, version 2.0.0; available from the corresponding author).[14] R-implemented scripts (R – statistical package) automatically detected the TDC-main peak

by a probability driven algorithm and fitted a generic double Gaussian model to that peak.[15] This unambiguously linked each absolute TTP-value ttp from the TDC to a distinct generic TDC_f -quantile z_f of the fitted model, which allowed optional switching between z_f- and corresponding absolute ttp-values. Thus, direct comparisons of different examinations were possible, as each z_f-value represents a unique point in the fitted model distribution TDC_f and thus indicates the same quantile in every DSC-examination. On the other hand, measurements of individually different hemodynamic aspects of a given DSC-examination still could be performed via the correlated absolute individual ttp-values.[1]

The TDC-main peak originates in the cascaded filling of the cerebral vessels during the first pass of the administered contrast bolus and is described by TDC_f. By separation of certain z_f-intervals from TDC_f, assumed to represent different vessel segments, the course of the hemodynamic characteristics of the bolus transit was investigated. According to a former study, the complete bolus transit includes all voxels defined in the interval

$$I_{AV} = \left\{ \mathrm{vxl} \mid -3 \le \mathrm{z_f}\left(\mathrm{ttp_{vxl}}\right) \le +3 \right\} \tag{1}$$

where vxl indicates the respective voxel with the absolute peak enhancement time $\mathrm{ttp_{vxl}}$ that is correlated to the TDC_f-quantile z_f.[1] The inflection points (IP) of TDC_f were considered to mark the transitions from large to small arterial (IP_a), and inversely, from small to large venous vessels (IP_v). IP_a and IP_v were consequently introduced as limits for the intervals

$$\begin{aligned} I_A &= \left\{ \mathrm{vxl} \mid -3 \le \mathrm{z_f}\left(\mathrm{ttp_{vxl}}\right) \le IP_a \right\} \quad \text{and} \\ I_V &= \left\{ \mathrm{vxl} \mid IP_v < \mathrm{z_f}\left(\mathrm{ttp_{vxl}}\right) \le +3 \right\} \end{aligned} \tag{2}$$

which include all voxels with a suitable $\mathrm{ttp_{vxl}}$ during the supposed arterial macro-vessel wash-in and the venous macro-vessel wash-out phase, respectively. The IPs were determined in TDC'_f, the first derivate of TDC_f, by numeric differentiation. Finally, the maximum of TDC_f, max_{TDCf}, supposed to mark the transition from arterioles to venules in the parenchyma, was used to additionally differentiate an arterial and a venous micro-vessel wash-in and wash-out phase

$$\begin{aligned} I_{art} &= \left\{ \mathrm{vxl} \mid IP_a \le \mathrm{z_f}\left(\mathrm{ttp_{vxl}}\right) \le max_{TDCf} \right\} \quad \text{and} \\ I_{ven} &= \left\{ \mathrm{vxl} \mid max_{TDCf} < \mathrm{z_f}\left(\mathrm{ttp_{vxl}}\right) < IP_v \right\} \end{aligned} \tag{3}$$

Note that max_{TDCf} is also the inflection point of the antiderivate of TDC_f, which represents the perfused total brain volume pTBV (unit: $\mathrm{cm^3}$) over time during the first pass of the bolus (Figure 2). The sum of pTBV and the volume of flagged unperfused voxels lying inside the brain parenchyma, provided automatically by the stdTTP-calculation, was taken as TBV. Additionally, an analysis of the whole arterio-venous transit interval I_{av}, with $I_{av} = I_{art} + I_{ven}$, was performed. The duration $\boldsymbol{T_I}$ of each interval $I = \{I_A, I_{av}, I_{art}, I_{ven}, I_V\}$ was then calculated as

$$\boldsymbol{T_I} = \mathbf{ttp}(z_f = \boldsymbol{u}_\mathrm{l}) - \mathbf{ttp}(z_f = \boldsymbol{l}_\mathrm{l}) \tag{4}$$

where ttp is the absolute peak enhancement time at the time-point defined by the TDC_f-quantile z_f, which corresponds either to the upper ($\boldsymbol{u}$) or the lower ($\boldsymbol{l}$) limit of the respective interval definition.

TDC_f showing the chronological change of pTBV per measured time step, where time step means the sequence repetition time TR was considered to model the velocity of the bolus spread or, simply, bolus spread velocity in the brain ($\boldsymbol{v}$, unit: $\mathrm{cm^3_{issue}/s^2/s}$). Consequently, mean $\bar{\boldsymbol{v}}_{\boldsymbol{I}}$ in each interval $\boldsymbol{I}$ was calculated as

$$\bar{\boldsymbol{v}}_{\boldsymbol{I}} = \boldsymbol{T_I}^{-1} \cdot \sum_{i=l}^{u} \mathrm{V_i} \quad \text{with} \quad \mathrm{V_i} = \left| \{ \mathrm{vxl} \,|\, \boldsymbol{z_f}(\mathrm{ttp_{vxl}}) = \boldsymbol{i} \} \right| \cdot \mathrm{V_{vxl}} \tag{5}$$

where $\mathrm{V_{vxl}}$ is the voxel-volume defined by the DSC-examination parameters, $\boldsymbol{u}$ and $\boldsymbol{l}$ are the upper and lower TDC_f-quantile limits and $\boldsymbol{T_I}$ is the duration of the respective interval I. Furthermore, as the first derivate of TDC_f displays the change of $\bar{\boldsymbol{v}}_{\boldsymbol{I}}$ over time, TDC'_f was considered to give the bolus spread acceleration ($\vec{\boldsymbol{a}}_{\boldsymbol{I}}$, unit: $\mathrm{cm^3_{tissue}/s^2}$), where mean $\bar{\boldsymbol{a}}_{\boldsymbol{I}}$ for every interval I was calculated as

$$\bar{\boldsymbol{a}}_{\boldsymbol{I}} = \boldsymbol{T_I}^{-1} \cdot \sum_{i=l}^{u} \frac{\Delta \mathrm{V_i}}{\mathrm{TR}} \tag{6}$$

where $\boldsymbol{T_I}$ and $\mathrm{V_i}$ are the same as in formulation 5, TR is the sequence repetition time, and $\Delta \mathrm{V_i}$ is the change of $\mathrm{V_i}$ per TR. Note that $\bar{\boldsymbol{a}}_{\boldsymbol{I}}$ typically shows negative values in the venous phases. The various interval durations as well as $\bar{\boldsymbol{v}}_{\boldsymbol{I}}$ and $\bar{\boldsymbol{a}}_{\boldsymbol{I}}$ for each interval I were calculated and compared between the three groups.

Statistical analysis

Quality of model fit was estimated by calculating $\mathrm{R^2}$ and the Spearman rank correlation coefficient ρ between TDC and TDC_f. Note that $\mathrm{R^2}$ is not simply ρ^2, but was calculated as

$$R^2 = 1 - \left(\sum_{z_f=-3}^{+3} \left(\mathrm{TDC}_{z_f} - TDC_{f_{z_f}} \right)^2 \cdot \left(\sum_{z_f=-3}^{+3} \left(\mathrm{TDC}_{z_f} - \overline{\mathrm{TDC}} \right)^2 \right)^{-1} \right)$$

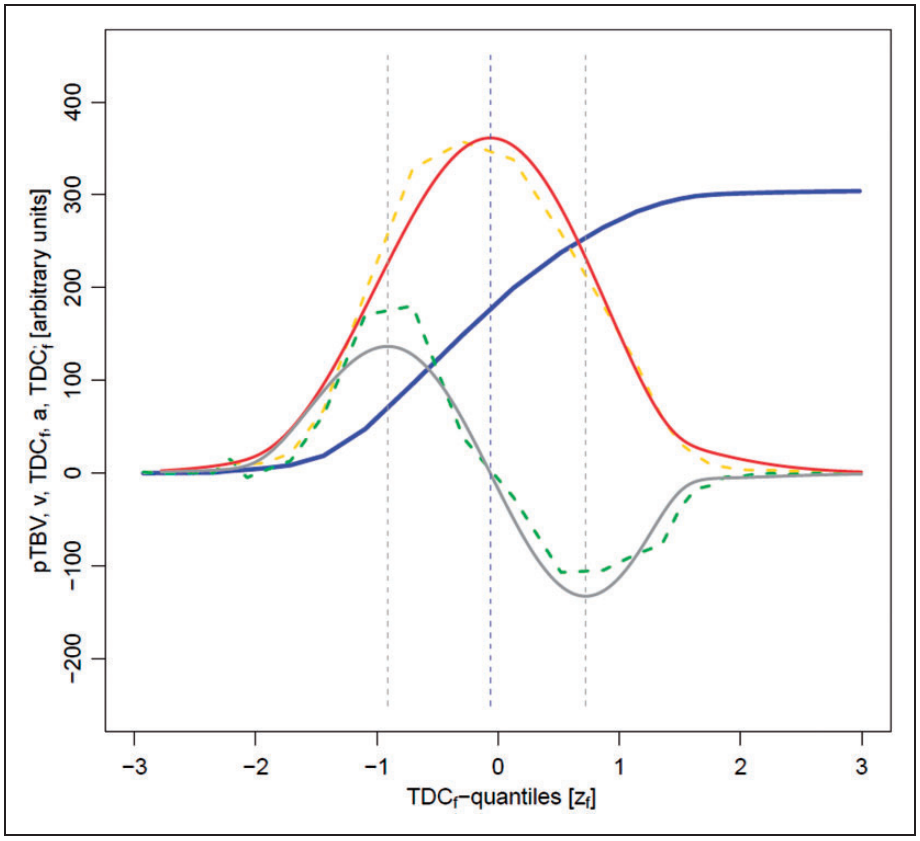

Figure 2. The TTP-histogram of a DSC-examination constitutes TDC (dashed yellow line), which was considered to show the bolus spread velocity v. Accordingly, its first derivate *TDC'* (dashed green line) relates to the bolus spread accelerations $\vec{a}$. Fitting a model to TDC provides TDC_f (solid red line), which is described by generic TDC_f-quantiles: z_f instead of absolute, but individually different, TTP-values and, thus, enables comparisons between different examinations. TDC_f predicts v and its first derivate TDC_f' (solid grey line) $\vec{a}$. The anti-derivate of TDC_f gives the volume–time curve (solid blue line) depicting the totally perfused volume over time. Inflection points of TDC_f (dashed grey lines) and its anti-derivate (dashed blue line) were used to classify different phases of the bolus transit.

where TDC refers to the TTP-histogram, TDC_f to the fitted double Gaussian model, and z_f to the TDC_f. quantiles.

Validity of nWMH-grouping and TCD-interval definition was visualised by creating cumulative maps showing the extent of nWMHs of the three groups and the location of the voxels included in the various TDC-intervals according to their z_f-value. Absolute measures of nWMHs and z_f-interval differences were further assessed statistically by group-level comparisons testing the whole microvascular arterio-venous transit, the micro-vessel arterial wash-in and the venous wash-out phase intervals I_{av}, I_{art} and I_{ven}, since only these intervals represented the parenchymal microvessels targeted in the study. Group-level comparisons were performed using Kruskal–Wallis (K–W) tests with Dunnett's Modified Tukey–Kramer Pairwise Multiple Comparison Test (DTK) as post hoc analysis to take potentially significant deviations from the normal distribution and inhomogeneity of variances, as well as the different size of the groups, into account. Correction for multiple comparisons was performed conservatively using the Bonferroni-method. Step-wise regression analysis was performed to explain dependencies of nWMH-volume using least trimmed squares and MM-estimation to treat outliers in the explanatory and responsive variables.[16]

Descriptive statistics are given as mean, SD or/and confidence intervals. Otherwise, if applicable, data are quoted as median, MAD or/and 95% percentiles. All TDC calculations and statistical evaluations were performed in R (version 3.2.0) invoking packages FlexMix, robustbase, vcd and DTK.[15–19]

Results

A summary of the demographic data of the three groups studied is given in Table 1. TBV was not significantly different between the three groups, and concerning age groups 1 and 2 were not significantly different as well (K-W test:TBV, age; $p > 0.05$). Also, testing $\boldsymbol{T_I}$, $\bar{\boldsymbol{v}}_{\boldsymbol{I}}$, and $\bar{\boldsymbol{a}}_{\boldsymbol{I}}$ for gender-related effects within and between

Table 1. Demographic data.

	Group 0 ($n = 18$)	Group 1 ($n = 38$)	Group 2 ($n = 50$)
Age (years)	$42.3 \pm 8.5^{*}$	68.4 ± 9.0	75.7 ± 9.6
Male/female††	9/9	19/19	33/17
Total brain volume (cm^3)	1400.2 ± 104.6	1408.9 ± 101.6	1398.1 ± 138.6
Normalised WMH-volume (cm^3)	10.4 ± 2.3	$17.1 \pm 5.5^{*}$	$52.1 \pm 17.7^{*}$
Hypertension	50%	65%	88%†
Diabetes	22%	32%	38%
Hyperlipidemia	50%	42%	58%
Smoking	17%	13%	18%

Note: Demographic data of group 0 (young controls), group 1 (elderly controls) and group 2 (cSVD-patients).
*Significantly different at $p < 0.01$.
†Significantly higher odds for risk factor at $p < 0.003$.
††No significant effect from gender within and between groups.

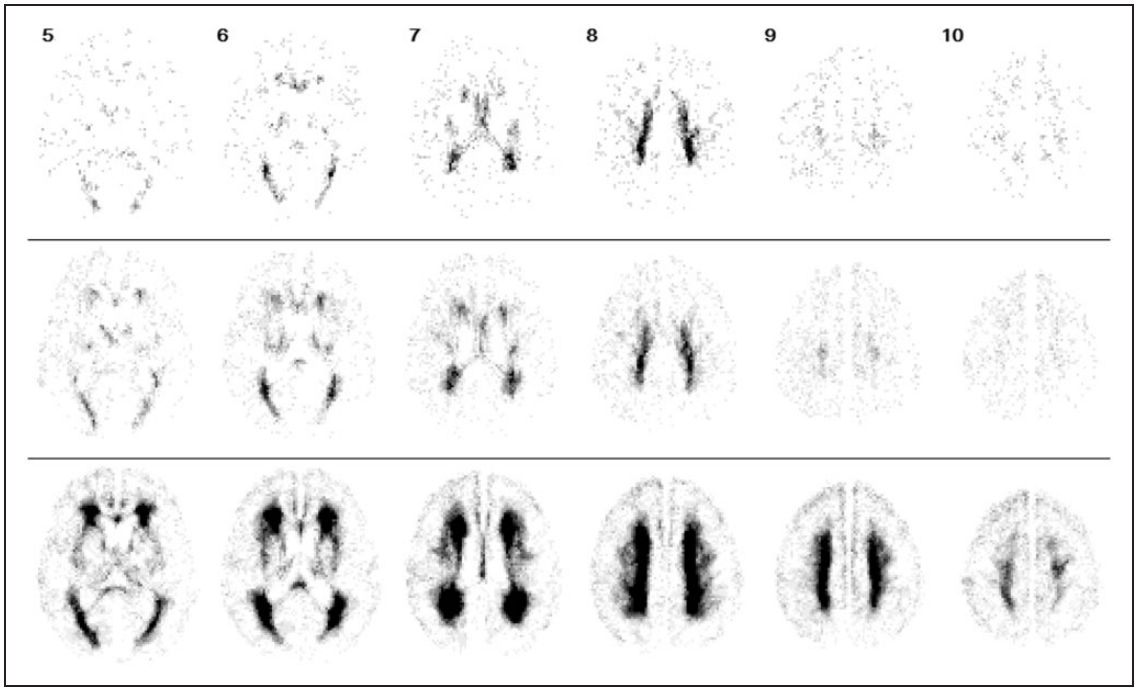

Figure 3. Normalised cumulative maps showing the extent of nWMHs (depicted as black areas) in the three different groups.: The nWMH-volume was significantly different between all three groups. Nevertheless visually, group 0 (top row; young controls, $n = 18$) was comparable to group 1 (middle row; elderly controls; $n = 38$), while in group 2 (bottom row; elderly cSVD-patients; $n = 50$) the cerebral white matter was severely affected by multiple confluent WMHs. Note that column-numbers given in the top row mark the same slices as in Figure 4.

groups (including cross-over testing female vs. male) in the various intervals was not significant despite the obvious predominance of male patients in group 2 (K–W test: $\boldsymbol{T_I}$, $\bar{\boldsymbol{v}}_{\boldsymbol{I}}$, $\bar{\boldsymbol{a}}_{\boldsymbol{I}}$ for $I = \{I_A, I_{av}, I_{art}, I_{ven}, I_V\}$ by gender; $p > 0.05$; post hoc: multiple t-tests; uncorrected). The odds to suffer from a certain risk factor were tested for groups 1 and 2, which were comparable concerning age. Here, only a significantly higher odds to suffer from hypertension was found in group 2 (odds-ratio test; group 1: [25+, 13−] vs group 2: [45+, 3−]; $p = 0.0028$).

The group-classification concerning the extent of WMHs was reviewed using cumulative maps, where, expectedly, group 0 and group 1 were visually comparable, while both groups exhibited clearly smaller WMH-volumes than group 3 (Figure 3). Nevertheless, in the statistical analysis, a significant difference between all three groups was obtained

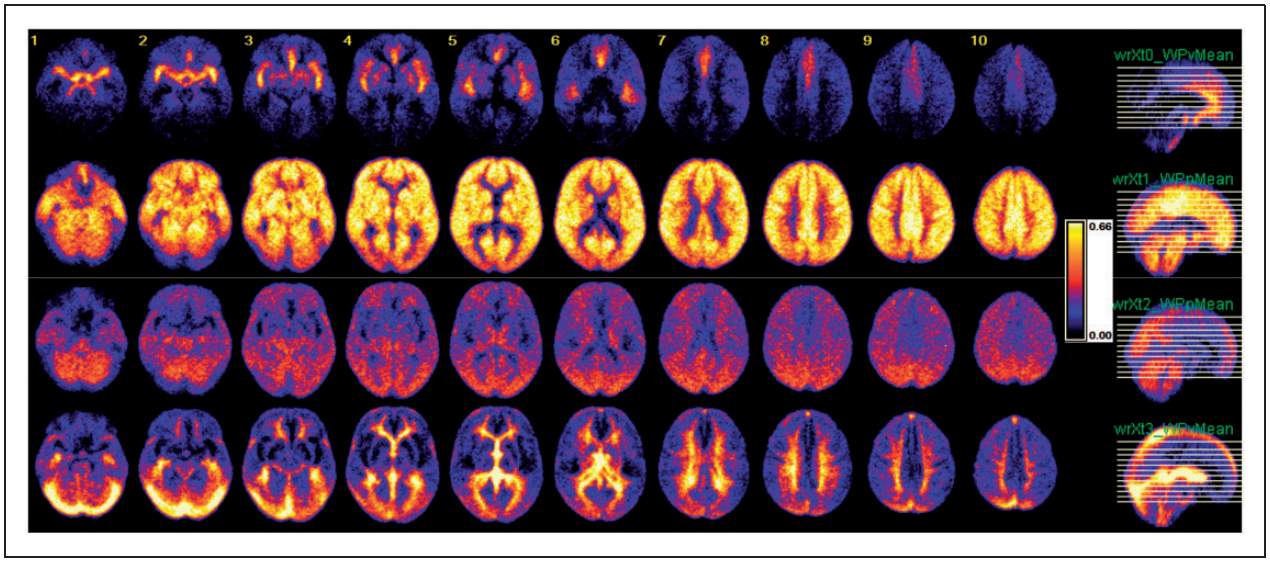

Figure 4. Normalised cumulative maps ($n = 106$) showing arterial macrovessel wash-in phase I_A (first row), the arterial microvessel wash-in phase I_{art} (second row), the venous microvessel wash-out phase I_{ven} (third row) and the venous macrovessel wash-out phase I_V (fourth row). The proposed TDC_f intervals provide an acceptable general description of the different phases of cerebral bolus transit. Note that column-numbers given in the top row mark the same slices as in Figure 3.

(K–W test: nWMH-volume; $p < 0.05$; post hoc: DTK; correction: Bonferroni). In the same way, validity of vessel segment classification based on TDC_f-quantiles $z_f = \{z_f(IP_a),\ z_f(max_{TDCf}),\ z_f(IP_v)\}$ was verified by cumulative maps showing the location of all voxels belonging to the respective intervals I_A, I_{art}, I_{ven}, and I_V, where the interval-definitions for I_{art} and I_{ven} effectively included the parenchymal microvessel segments (Figure 4). The quality of the model fit was excellent with $\rho = 0.992$ (Spearman; 95% interval: 0.965–0.997) and $R^2 = 0.985$ (95% interval: 0.882–0.996).

The evaluation of the bolus transit duration $\boldsymbol{T_I}$ in the intervals I_{av}, I_{art}, and I_{ven} showed a significant prolongation of $\boldsymbol{T_{av}}$ for the whole transit period I_{av} as well as for the arterial microvessel wash-in phase I_{art} when comparing group 2 to the control-groups 0 and 1, while group 0 was not different to group 1 (K–W test: $\boldsymbol{T_{av}}$, $\boldsymbol{T_{art}}$; $p < 0.05$; post hoc: DTK; correction: Bonferroni). In the venous microvessel wash-out phase, a significant difference was detected only between group 0 and group 2 (K–W test: $\boldsymbol{T_{ven}}$; $p < 0.05$; post hoc: DTK; correction: Bonferroni). The range of all durations in the control groups measured for the whole interval I_{av}, which represents the global parenchymal arterio-venous bolus transit time, was 3.7 ± 1.1 s (median $\pm$ MAD; range: 2.2–8.9 s). In the cSVD-group 2, this interval duration was 4.4 ± 1.1 s (median $\pm$ MAD; range: 3.0–7.4 s). The transit duration $\boldsymbol{T_A}$ representing the wash-in phase of cerebral macrovessels was not significantly different between the various groups (K–W test: $\boldsymbol{T_A}$; $p > 0.05$; post hoc: DTK; correction: Bonferroni).

For $\bar{\boldsymbol{v}}_{\boldsymbol{I}}$ and $\bar{\boldsymbol{a}}_{\boldsymbol{I}}$, significant differences between both control groups, 0 and 1, and group 2 were found for all intervals I_{av}, I_{art} and I_{ven}. Yet, in the specified intervals, no significant differences were found between the two control groups (K–W test: $\bar{\boldsymbol{v}}_{\boldsymbol{I}=\{I_{av}, I_{art}, I_{ven}\}}$, $\bar{\boldsymbol{a}}_{\boldsymbol{I}=\{I_{av}, I_{art}, I_{ven}\}}$; $p < 0.001$; post hoc: DTK; correction: Bonferroni). A full summary of all group comparisons is given in Table 2.

A scatter analysis of $\bar{\boldsymbol{v}}_{\boldsymbol{av}}$ in relation to $\boldsymbol{T_{av}}$ using robust regression analysis suggests an exponential correlation between both variables. The regression lines of the control groups 0 and 1 show a broad overlap with cSVD-group 2 at the point ($282.4\,cm^3_{tissue}/s$, 3.4 s). Remarkably, below this intersection point with decreasing $\bar{\boldsymbol{v}}_{\boldsymbol{av}}$, the duration $\boldsymbol{T_{av}}$ increased clearly faster in group 2 than in both control groups, i.e. 0 and 1. Investigating the scatter and correlation of $\bar{\boldsymbol{v}}_{\boldsymbol{av}}$, directly depicted by TDC, and nWMH volume also revealed an indirect exponential correlation between both variables in robust regression analysis. Median and MAD in group 2 were $212.2 \pm 48.7\,cm^3_{tissue}/s$ for $\bar{\boldsymbol{v}}_{\boldsymbol{av}}$ and $48.3 \pm 14.7\,cm^3$ for nWMH-volume, which enables to estimate a $\bar{\boldsymbol{v}}_{\boldsymbol{av}}$-range, where $\bar{\boldsymbol{v}}_{\boldsymbol{av}}$-values in the control-groups widely matched those of the cSVD-group. However, in this range in controls, at least in our sample, WMHs were not yet evident in T2-weighted MRI (Figure 5).

Finally, we performed robust regression analysis explaining the extent of nWMH-volume by $\bar{\boldsymbol{v}}_{\boldsymbol{av}}$ with a step-wise inclusion of other relevant confounders of nWMH. Improvement of the model by each inclusion-step was tested using analysis of variance, where no significant improvement or effect was found

Table 2. Results from TDC analysis.

Both groups 0 ($n = 18$) and 1 ($n = 38$) different from group 2 ($n = 50$): *$p < 0.05$; **$p < 0.01$	Interval I_{av} (I_{art}+I_{ven})	Interval I_{art}	Interval I_{ven}
Group $0_{controls\ young}$	284.3 ± 52.6	302.3 ± 59.0	266.4 ± 52.9
Group $1_{controls\ elderly}$	257.6 ± 53.3	267.8 ± 58.2	247.3 ± 51.7
Group $2_{cSVD\ elderly}$ _	211.9 ± 44.0**	215.2 ± 51.0**	208.6 ± 44.4**
Bolus spread velocity v [$cm^3_{issue}/s^2/s$]			
Group $0_{controls\ young}$	85.3 ± 25.5	105.6 ± 39.9	65.0 ± 26.7
Group $1_{controls\ elderly}$	67.2 ± 32.7	82.6 ± 43.6	51.9 ± 26.9
Group $2_{cSVD\ elderly}$ _	44.0 ± 24.3**	55.7 ± 30.2**	30.3 ± 27.3**
Bolus spread acceleration $\vec{a}$ cm^3_{issue}/s^2			
Group $0_{controls\ young}$	3.3 ± 0.6	1.6 ± 0.4	1.6 ± 0.3
Group $1_{controls\ elderly}$	3.7 ± 1.1	1.9 ± 0.6	1.8 ± 0.6 _
Group $2_{cSVD\ elderly}$ _	4.4 ± 1.1	2.2 ± 0.6*	2.1 ± 0.6*
Bolus transit time T_I [s]			

Note: $\boldsymbol{T}$, v and $\vec{a}$ derived from DSC measurements during the intervals I_{av}, I_{art} and I_{ven} (*$p < 0.05$; **$p < 0.01$). All analyses were corrected for different group sizes, heteroscedasticity and multiple comparisons. Note that $\vec{a}_{ven}$ in I_{ven} (wash-out phase) is negative, however, the absolute values are given.

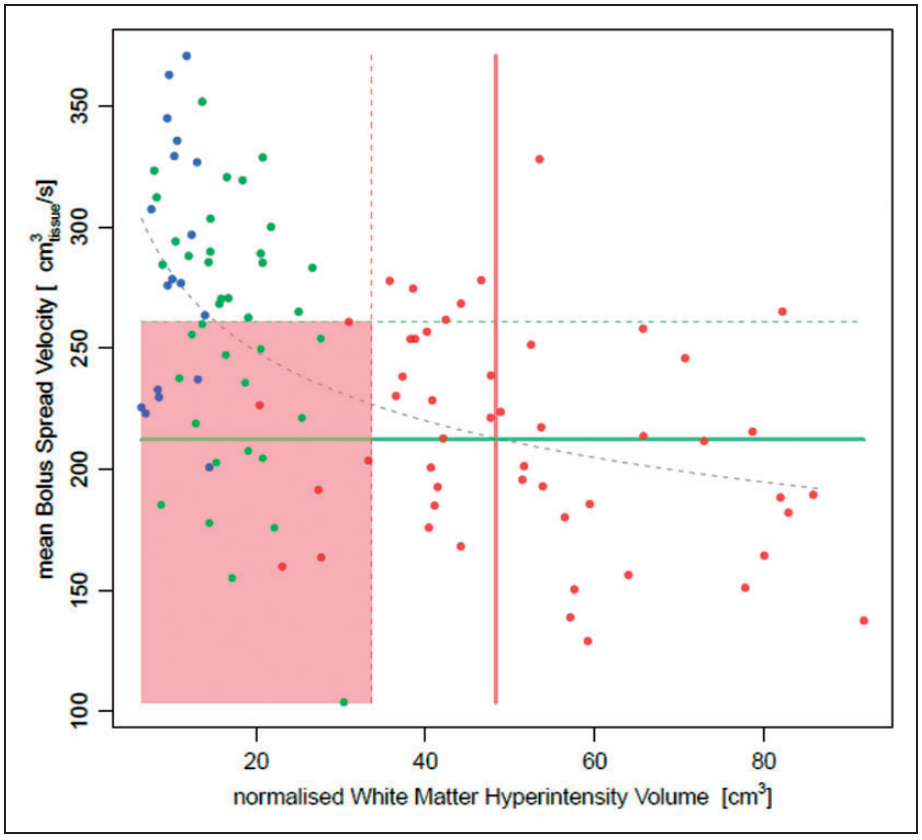

Figure 5. Bolus spread velocity $\bar{v}_{av}$ and normalised white matter hyperintensity volume nWMH-V showed an indirect exponential correlation (dashed grey regression line). The scattering of both variables in group 2 (red dots), when described by robust statistics (median [horizontal green and vertical red solid lines] ± MAD [horizontal green and vertical red dashed lines]), suggests a certain $\bar{v}_{av}$-range where below cSVD is most likely but WMHs may not yet have developed (red shaded area). Note that 41% of the control patients (group 0: 6 cases, 33.3%; group 1: 17 cases, 44.7%) were within this range. Blue and green dots mark cases of young and elderly controls, represented in groups 0 and 1, respectively.

for: gender, diabetes, hyperlipidemia and smoking (ANOVA, $p > 0.05$ n.s.). The base model (nWMH by $\bar{v}_{av}$) showed an adjusted-R^2 of 0.2696 ($p < 0.001$). The strongest confounding effect was obtained for age (nWMH by $\bar{v}_{av}$+age; adjusted-$R^2 = 0.5766$; $p < 0.001$), while hypertension exhibited a non-significant, weak effect on the model (nWMH by $\bar{v}_{av}$+age+hypertension; adjusted-$R^2 = 0.5808$; $p = 0.1168$ n.s.).

Discussion

Investigating TTP-histograms, dubbed TDC, derived from established DSC-MRI, we found striking evidence that a substantial part of the hemodynamic alterations detected by the TDC may directly arise from modifications in the cerebral microvascular bed. The evaluation of the bolus transit dynamics in cerebral parenchyma revealed an exponential decrease of the TDC-derived mean bolus spread velocity $\bar{v}_{av}$ in cerebral parenchyma, when the normalised volume of cerebral WMHs, primarily attributable to cSVD, increased. The concomitant delay in the filling of the various vessel segments, documented as a significant reduction of the bolus volume acceleration $\bar{a}_I$ during the parenchymal wash-in phase in patients with clear signs of cSVD, also suggests a microvascular modification that seems to restrict the general bolus spread in the brain over time. This finding matches recently discussed theories about cSVD, where diffuse endothelial failure in cerebral microvessels was postulated as an early stage of the disease. Not until microvascular degeneration causes critical ischemia by luminal narrowing or occlusion of severely affected vessels, however, focal infarctions and, consecutively, WMHs occur.[4] Immediate effects from cSVD would therefore stay undetectable in conventional MRI pending an ischemic event triggered by the postulated endothelial failure. In this context, an animal experiment in rats prone to microangiopathy revealed that histologically proven microvessel wall alterations led to accumulations of erythrocytes with stasis of blood flow in capillaries in the early stage of disease, which were not detectable from conventional high-resolution 3T MRI.[20] Though this remains to be proven in humans, at this stage, when temporary stasis of capillary flow is the major impairment caused by cSVD, the only alteration measureable in MRI would most probably be a prolongation of the arterio-venous transit time. Actually, this was found in TDC-measurements, which also complies with the known reduction of regional cerebral blood flow not only in WMHs, but also in unaffected white matter in patients with cSVD documented by DSC-MRI and pulsed arterial spin labelling measurements.[21,22] Prior to this, another study demonstrated histologically the reduction of the cerebral vessel density not only in WMHs but also in normal appearing white matter in cSVD-patients.[12] Consequently, endothelial degeneration, eventually followed by loss of capillaries, may be understood as a chronic process and the vascular impairment itself seems to take place long before WMHs become detectable via MRI. This conforms to our finding that $\bar{v}_{av}$ values overlap between all groups in the range below app. 261–282 cm^3/s, where about 41% of controls exhibited nearly no WMHs and patients in group 2 show clearly visible WMHs (Figure 5). Thus, considering cases with a normal appearing white matter and a low $\bar{v}_{av}$ to be at risk for cSVD, estimation of $\bar{v}_{av}$ via the TDC could open a novel approach to investigate cSVD clearly before WMHs become manifest at a stage where microvascular degeneration is less progressed and probably more susceptible to medical treatment.[23] Of course, this has to be investigated and proven in future prospective studies. On the other hand, the TDC-findings are in full agreement with earlier reports also using DSC-MRI on this topic, where a reduction of regional cerebral blood flow in normal appearing white matter was described.[21,24] However, assessment using TDC appears much more robust since there is no need for an arterial input function (AIF) or an adjustment to prior positron emission tomography measurements when simply evaluating the TDC.[1,21,24] Moreover, comparisons between positron emission tomography and DSC-MRI using an AIF for perfusion assessment showed a considerable dependency of calculated parameter values on the location of the AIF.[25]

In a conceivable cascade of endothelial failure, perfusion impairment and loss of capillaries, quasi as a subsequent feature in the course of cSVD, arteriolar tortuosity and venous collagenosis were also reported to deteriorate microvascular flow and, therefore, to reinforce the effect from initial endothelial failure. Despite the fact that the exact relationship between these findings and cSVD is discussed controversially, a histologically visible loss of white matter cellular components was proven in all patients in the respective study, where the authors themselves stated that: "…. *Only the very largest of these lesions might be detected on MRI scans, ….*"[26] This underlines our proposal to rather focus TDC-evaluations on patients of groups 0 and 1 who present with a drop of $\bar{v}_{av}$ and a prolongation of T_{av}. In this setting, persons potentially suffering from cSVD would most probably remain undetected in any investigation relying on visual WMH-scoring only, but could be detected assessing the TDC.

Importantly, our results suggest that microangiopathic flow impairment is sensitively reflected by the increase in T_{av} and a decrease of $\bar{v}_{av}$, since both parameters would respond this way to a reduction of the active microvascular cross-section that is available for tissue perfusion. This also perfectly agrees with

measurements comparable to the TDC-interval I_{av} performed using contrast-enhanced transcranial Doppler sonography, where the means for the transit times in patients with cSVD where reported ranging from 4.4 s to 6.7 s, and for controls or patients with neurodegenerative disease, a regular range of 1.3–3.7 s was measured.[27,28] Similarily, TDC-derived transit times were 3.3–3.7 s for controls and 4.4 s for cSVD-patients in our study, limited of course by the lower temporal resolution of MRI. Therefore, the generic bolus passage interval classification based on TDC_f-quantiles z_f proves to be valid, which is also supported by the excellent correlations between the raw TDC and the fitted model TDC_f. Hence, $\boldsymbol{T_{av}}$ directly calculated from TDC_f is a reliable measure of the arterio-venous transit time. Because all DSC-derived hemodynamic perfusion time parameters were shown to directly depend on the arterio-venous transit time, $\boldsymbol{T_{av}}$, that is directly available from the respective DSC-MRI examination, it could be useful to either correct the parameter or the associated critical perfusion-threshold for individually different degenerative microvascular adaptions in order to obtain more robust predictions of the infarct core in acute stroke.[1–3] Given that our results strongly suggest microvascular flow impairment as the major source for variations of $\boldsymbol{T_{av}}$, the consideration to adapt measurements to an intrinsic threshold rather than to a global one gets even more important as the possibility was stressed that capillary flow itself may generally be rather heterogeneous.[29] Moreover, besides gender, severe WMHs attributable to cSVD were also realised as an independent predictor for infarct size in acute ischemic stroke, where additionally a controversially discussed coincidence between a prolongated filling of collaterals, also important in acute stroke, and a larger extent of WMHs was reported.[30–32] In any case, further prospective studies on this topic will be needed.

However, we also acknowledge certain limitations. Vascular risk factors and certain properties of those, such as duration and severity, could not be assessed specifically and we neither aimed to measure their effects on cerebral hemodynamics nor did we intend to relate hemodynamic findings with clinical manifestations caused by cSVD. Our investigation focused rather on the grade of hemodynamic alterations potentially caused by modifications in the microvascular bed due to any reason for cSVD in order to expand diagnostic capabilities of DSC-MRI. Despite this, the frequencies of the various risk factors in the respective groups were widely comparable, except for hypertension, which was more frequently found in group 2. Anyway, including hypertension into the model did not improve the model significantly, while age did. This poses the question whether patients at higher age often share a longer duration of cerebrovascular disease, which in turn increases the possibility for a higher nWMH-volume. On the other hand, relatively low nWMH-volumes in older patients could be very well explained by a late onset of cSVD. Interestingly, the only severe outlier from the model was an 80-year-old woman who presented with multiple recently discovered risk factors and a low nWMH-volume, but showed a clear decrease of $\bar{\boldsymbol{v}}_{\boldsymbol{av}}$. However, since our study lacks longitudinal time information, further studies on this topic will be needed. Additionally, a considerable influence from reduced cardiac output on the shape of the TDC was not assessed explicitly, since patients with severe cardiac failure were not included in the study and a previous thorough analysis of major aspects of the central circulatory bolus spread in the heart and lungs showed only a weak influence from a reduced left ventricular ejection fraction on the bolus shape.[33]

Also, we used an unbiased fully automatic segmentation algorithm that was designed to yield classifications comparable to the visual scores proposed by the LADIS study.[10,11] Yet, patients of group 0 were to some extent assigned visually from the distribution of the nWMH-volumes to define the base-line. While this did not completely exclude an inclusion-bias in group 0, where bias should be lowest, this was quite avoided in groups 1 and 2. Though this has to be validated further in larger samples, differentiation of cSVD from controls seems acceptable in this study, which could be demonstrated by the cumulative maps depicting the extent of WMHs of the different groups. The automatic classification assigned grade 1 to group 0, group 1 resembled very much grade 2, and group 2 fitted grade 3, according to visual scoring as proposed in the literature.[10,11] Note also that extracting patients from a hospital database per se widely precludes inclusion of truly healthy persons. Thus, it has to be emphasised that our groups 0 and 1, used as controls, rather represent the lowest grade of cSVD detectable, which is a common limitation found in trials investigating cSVD. Nonetheless, direct comparisons of our results with those from other studies based on pure visual scoring should be done very carefully.

Furthermore, our study lacks an age-matched group of younger patients with severe WMH-manifestations, which is widely owed to the fact that hereditary vasopathies were excluded. Nevertheless, in a sonographic study, the hemodynamic impairment in younger patients suffering a hereditary vasopathy was comparable to group 3 in our sample.[27,28] Thus, we do not expect a significant effect on our results.

Finally, gender is known to show an effect on cerebral perfusion.[34] While groups 0 and 1 contained equal numbers of male and female patients, in group 2 predominantly male patients were represented. Multiple comparisons between male and female

subgroups within and between groups including cross-over testing (i.e. male vs. female) did not reveal any effect from gender differences in our sample. This could result from the fact that TDC evaluates the global cerebral bolus transit, which might turn out as more robust to this confounding effect than the voxel-wise evaluations usually performed. It is important to note that age, also yielding a strong effect on both transit time and nWMH-volume, was comparable between groups 1 and 2. This additionally underlines a strong effect from presumably microvascular alterations on the measured differences of cerebral hemodynamics between these groups.

In conclusion, our findings support the hypothesis of a direct relationship between the extent of normalised WMH-volume, attributable to underlying cSVD, and its presumably direct influence on the arterio-venous transit time measured by TDC derived from DSC-MRI. This is of great interest since, on the one hand, TDC could be used to support further adjustment of the DSC-MRI derived perfusion time parameters, which depend on the arterio-venous transit time. On the other hand, TDC could provide a novel approach to robust assessment of early cSVD. As a future prospect, our approach could provide a more accurate analysis of early stages of cSVD that might help to improve therapeutical treatment.

Funding

The author(s) disclosed receipt of the following financial support for the research, authorship, and/or publication of this article: This work was financially supported in part via a grant from the Austrian Science Fund (FWF P23533-B13) and an unrestricted grant to E.M. by Siemens Medical Solutions, Austria. Parts of the data were presented at ESMRMB 2015.

Declaration of conflicting interests

The author(s) declared the following potential conflicts of interest with respect to the research, authorship, and/or publication of this article: Christian Nasel received lecture and consulting fees from Bracco and Guerbet, both unrelated to this study. All other authors declare no conflict of interest.

Authors' contributions

NC contributed to preparation of the paper, MR measurements and data evaluation; BRN and KK contributed to preparation of the paper and data evaluation; and ME contributed to preparation of the paper and final approval of the manuscript.

Statement on underlying research materials

All underlying research materials related to our paper can be accessed anonymously upon request. Otherwise, all relevant data are included in the manuscript.

References

1. Nasel C, Kalcher K, Boubela R, et al. Improved quantification of cerebral hemodynamics using individualized time thresholds for assessment of peak enhancement parameters derived from dynamic susceptibility contrast enhanced magnetic resonance imaging. *PLoS ONE* 2014; 9: e114999.
2. Yamada K. Magnetic resonance perfusion-weighted imaging of acute cerebral infarction: effect of the calculation methods and underlying vasculopathy. *Stroke* 2002; 33: 87–94.
3. Ibaraki M, Ito H, Shimosegawa E, et al. Cerebral vascular mean transit time in healthy humans: a comparative study with PET and dynamic susceptibility contrast-enhanced MRI. *J Cerebral Blood Flow Metab* 2006; 27: 404–413.
4. Wardlaw JM, Smith C and Dichgans M. Mechanisms of sporadic cerebral small vessel disease: insights from neuroimaging. *Lancet Neurol* 2013; 12: 483–497.
5. True Random Number Service. http://www.random.org
6. World Medical Association - Declaration of Helsinki. http://www.wma.net/en/30publications/10policies/b3/
7. Nasel C. Protoneus-sequence: extended fluid-attenuated inversion recovery MR imaging without and with contrast enhancement. *Eur J Radiol* 2005; 55: 219–223.
8. Nasel C, Azizi A, Veintimilla A, et al. A standardized method of generating time-to-peak perfusion maps in dynamic-susceptibility contrast-enhanced MR imaging. *AJNR Am J Neuroradiol* 2000; 21: 1195–1198.
9. Greitz D. Radiological assessment of hydrocephalus: new theories and implications for therapy. *Neurosurg Rev* 2004; 27: 145–165.
10. Fazekas F, Chawluk JB, Alavi A, et al. MR signal abnormalities at 1.5 T in Alzheimer's dementia and normal aging. *AJR Am J Roentgenol* 1987; 149: 351–356.
11. Pantoni L, Basile AM, Pracucci G, et al. Impact of age-related cerebral white matter changes on the transition to disability – the LADIS study: rationale, design and methodology. *Neuroepidemiology* 2005; 24: 51–62.
12. Moody DM, Thore CR, Anstrom JA, et al. Quantification of afferent vessels shows reduced brain vascular density in subjects with leukoaraiosis. *Radiology* 2004; 233: 883–890.
13. Rorden C and Brett M. Stereotaxic display of brain lesions. *Behav Neurol* 2000; 12: 191–200.
14. Nasel C, Kronsteiner N, Schindler E, et al. Standardized time to peak in ischemic and regular cerebral tissue measured with perfusion MR imaging. *AJNR Am J Neuroradiol* 2004; 25: 945–950.
15. R-Development CoreTeam. R: A Language and Environment for Statistical Computing. In: R Foundation for Statistical Computing (ed.) *R version 3.11.0. (2015-04-16)*, Vienna, Austria. 2015. ISBN 3-900051-07-0.
16. Rousseeuw P, Croux C, Todorov V, et al. robustbase: Basic Robust Statistics. R package version 0.92-5, http://CRAN.R-project.org/package = robustbase (2014 accessed 17 June 2015).

17. Gruen B and Leisch F. FlexMix Version 2: Finite mixtures with concomitant variables and varying and constant parameters. *J Stat Software* 2008; 28: 1–35.
18. Lau MK. DTK: Dunnett–Tukey–Kramer pairwise multiple comparison test adjusted for unequal variances and unequal sample sizes. R package version 3.5, http://CRAN.R-project.org/package=DTK (2015; accessed22 June 2013).
19. Meyer D, Zeileis A and Hornik K. vcd: Visualizing Categorical Data. In. R package version 1.4-1 ed, 2015.
20. Mencl S, Garz C, Niklass S, et al. Early microvascular dysfunction in cerebral small vessel disease is not detectable on 3.0 Tesla magnetic resonance imaging: a longitudinal study in spontaneously hypertensive stroke-prone rats. *Exp Transl Stroke Med* 2013; 5: 8.
21. Markus HS, Lythgoe DJ, Ostegaard L, et al. Reduced cerebral blood flow in white matter in ischaemic leukoaraiosis demonstrated using quantitative exogenous contrast based perfusion MRI. *J Neurol Neurosurg Psychiatr* 2000; 69: 48–53.
22. Bastos-Leite AJ, Kuijer JPA, Rombouts SARB, et al. Cerebral blood flow by using pulsed arterial spin-labeling in elderly subjects with white matter hyperintensities. *Am J Neuroradiol* 2008; 29: 1296–1301.
23. Ebinger M, Brunecker P, Schultze-Amberger J, et al. Statins and cerebral perfusion in patients with leukoaraiosis - a translational proof-of-principal MRI study. *Int J Stroke* 2012; 7: E5–E5.
24. O'Sullivan M, Lythgoe DJ, Pereira AC, et al. Patterns of cerebral blood flow reduction in patients with ischemic leukoaraiosis. *Neurology* 2002; 59: 321–326.
25. Zaro-Weber O, Moeller-Hartmann W, Heiss WD, et al. Influence of the arterial input function on absolute and relative perfusion-weighted imaging penumbral flow detection: a validation with (1)(5)O-water positron emission tomography. *Stroke* 2012; 43: 378–385.
26. Brown WR, Moody DM, Challa VR, et al. Venous collagenosis and arteriolar tortuosity in leukoaraiosis. *J Neurol Sci* 2002; 203-204: 159–163.
27. Puls I, Hauck K, Demuth K, et al. Diagnostic impact of cerebral transit time in the identification of microangiopathy in dementia: A transcranial ultrasound study. *Stroke* 1999; 30: 2291–2295.
28. Liebetrau M, Herzog J, Kloss CU, et al. Prolonged cerebral transit time in CADASIL: a transcranial ultrasound study. *Stroke* 2002; 33: 509–512.
29. Jespersen SN and Østergaard L. The roles of cerebral blood flow, capillary transit time heterogeneity, and oxygen tension in brain oxygenation and metabolism. *J Cerebral Blood Flow Metab* 2011; 32: 264–277.
30. Henninger N, Lin E, Haussen DC, et al. Leukoaraiosis and sex predict the hyperacute ischemic core volume. *Stroke* 2013; 44: 61–67.
31. Sanossian N, Ovbiagele B, Saver JL, et al. Leukoaraiosis and collaterals in acute ischemic stroke. *J Neuroimag* 2011; 21: 232–235.
32. Villringer K, Serrano-Sandoval R, Grittner U, et al. Subtracted dynamic MR perfusion source images (sMRP-SI) provide collateral blood flow assessment in MCA occlusions and predict tissue fate. *Eur Radiol* 2016; 26: 1396–1403.
33. Kreitner KF, Kunz RP, Weschler C, et al. Systematische Analyse der Geometrie eines definierten Kontrastmittelbolus - Implikationen für die kontrastmittelverstärkte 3D-MR-Angiographie thorakaler Gefäße. *RöFo – Fortschritte auf dem Gebiet der Röntgenstrahlen und der bildgebenden Verfahren* 2005; 177: 646–654.
34. Shin W, Horowitz S, Ragin A, et al. Quantitative cerebral perfusion using dynamic susceptibility contrast MRI: Evaluation of reproducibility and age- and gender-dependence with fully automatic image postprocessing algorithm. *Magnet Resonance Med* 2007; 58: 1232–1241.